AIAA JOURNAL
Vol. 41, No. 8, August 2003

# Spring-Supported Cylinder Wake Control

M. M. Zhang,* Y. Zhou,† and L. Cheng‡
*Hong Kong Polytechnic University, Kowloon, Hong Kong, People's Republic of China*

**A novel technique is proposed for the vortex control in the wake of a freely vibrating bluff body. The essence of the technique is to create a local perturbation on the surface of the body using piezoelectric actuators, thus modifying interactions between the flow and the structure. A square cylinder, flexibly supported on springs at both ends, was placed in a uniform flow and allowed to vibrate laterally. Three actuators were embedded underneath one side, parallel to the flow, of the cylinder. They were simultaneously activated by a sinusoidal wave, thus causing the cylinder surface to oscillate. Measurements were conducted at the synchronization condition when the vortex shedding frequency $f_s$ coincided with the natural frequency of the fluid-structure system. As the perturbation frequency $f_p$ of the actuators falls in the synchronization range, both particle image velocimetry and laser-induced fluorescence flow visualization captured dramatically enhanced vortices shed from the cylinder. The circulation of these enhanced vortices doubled. On the other hand, when $f_p$ was shifted away from the synchronization the vortex circulation dropped by about 50%. The spectral analysis of the structural displacement signal $Y$ and hot-wire signal $u$ points to the fact that the perturbation has altered fluid-structure interactions, the spectral phase $\phi_{Yu}$ at $f_s$ between fluid excitation and structural vibration changing from 0 to $-\pi$, namely, from reinforcing each other to dissipating each other. The perturbation effect on the drag coefficient and the crossflow distribution of Reynolds stresses is also investigated.**

## I. Introduction

FLUID flowing over a bluff body is a common occurrence. Examples include flow past heat exchangers, offshore structures, power transmission lines, and high-rise buildings. When the Reynolds number $Re$ exceeds a critical value, the boundary layer will separate from the body to form an unsteady flow pattern, that is, a staggered vortex street. In engineering, the unsteady flow pattern around the body often needs altering, either cancelled, for example, to suppress flow-induced vibration, or reinforced such as for transport enhancement in heat-transfer applications. The vortex control problem has therefore attracted a great deal of interest in the past.

The vortex control strategy can be passive or active. A passive method requires no energy input, thus having the advantage of being easier to implement, less expensive in cost, and more stable. Previous passive approaches frequently rely on adding surface protrusions, shrouds, or near-wake stabilizers to the structures to modify vortex shedding. The methods have proved successful particularly in offshore explorations and marine hydraulics.

The active control strategy can be separated into open- and closed-loop control. A closed-loop active control system uses actuators driven by external energy sources through a feedback-signal controlled electronic system. The action of the actuators alters fluid or structural dynamics or interactions between the two nonlinear dynamical systems, thus counteracting the effect of the flow instability. Berger[1] was probably the first to introduce the feedback control to suppress the wake instability. He used a hot-wire signal obtained in the wake to actuate a bimorph cylinder and reported the possibility of avoiding vortex shedding at a low Reynolds number $Re \equiv U_\infty h/\nu = 80$, where $U_\infty$ is the freestream velocity, $h$ is the characteristic height of the cylinder, and $\nu$ is the kinematic viscosity. Warui and Fujisawa[2] managed to reduce the vortex strength using electromagnetic actuators installed at both ends of a circular cylinder to create a lateral oscillation, which was controlled by a feedback hot-wire signal from the turbulent wake ($Re = 6.7 \times 10^3$). Fujisawa et al.[3] and Fujisawa and Nakabayashi[4] introduced a rotational oscillation and used different feedback control algorithms to reduce effectively velocity fluctuations and drag force ($Re = 2 \times 10^4$). The cylinder was activated by the hot-wire feedback signal from fluctuating velocities in the wake. Using a similar oscillation method, Tokumaru and Dimotakis[5] managed to attenuate both vortex strength and drag force ($Re = 1.5 \times 10^4$). Shiels and Leonard[6] investigated numerically the physics underlying Tokumaru and Dimotakis's observation and concluded that rotational oscillation triggered multiple vorticity structures, which lead to a time-averaged separation delay and subsequently drag reduction. Baz and Ro[7] used an electromagnetic actuator installed inside a cylinder to exert a force on the cylinder. The actuator was driven by a feedback hot-wire signal measured in the wake, thus increasing damping to the cylinder and effectively reducing the vortex-induced vibration at the occurrence of resonance, when the vortex shedding frequency $f_s$ coincided with the natural frequency $f_n'$ of the system. One common feature in these investigations is to alter the structural dynamics, subsequently influencing the flowfield.

Another approach is to use acoustic excitation to control the flowfield. Ffowcs-Williams and Zhao[8] used a hot-wire signal to provide a feedback control into a loudspeaker mounted on the wind-tunnel wall. The acoustic excitation from the loudspeaker suppressed vortex shedding from a cylinder ($Re = 4 \times 10^2$). Roussopoulos[9] revisited the investigation and concluded that the onset Reynolds number for vortex shedding could be increased by 20% as a result of the control. Lewit[10] used a feedback hot-wire signal to activate sound waves inside a circular tube. The sound waves interacted with flow through two rows of holes, arranged at ±90 deg away from the forward stagnation line of the tube, respectively, so that the sound waves through the two rows of holes were in antiphase, thus suppressing vortex shedding from the tube up to $Re = 10^4$. Huang[11] also introduced sound, again generated inside a cylinder and activated by a feedback hot-wire signal from the wake, into flow through a thin slit on the cylinder surface. He found that the shear flow near the slit was modified so that vortex shedding could be suppressed up to a Reynolds-number range between $4 \times 10^3$ and $1.3 \times 10^4$. Both Lewit and Huang applied a high level of acoustic excitation (more than 120 dB) in order to produce sufficient control effects. This might not be a feasible solution when noise is a concern.

In contrast with the closed-loop control, an open-loop control injects energy to the system without a feedback loop. Williams et al.[12]

Received 20 August 2002; revision received 13 December 2002; accepted for publication 23 February 2003. 

*Ph.D. Candidate, Department of Mechanical Engineering, Hung Hom.
†Associate Professor, Department of Mechanical Engineering, Hung Hom.
‡Professor, Department of Mechanical Engineering, Hung Hom.

introduced symmetric and antisymmetric acoustic excitations into a water flow ($Re = 470$) at a frequency of about $2f_s$ through two rows of holes located at $\pm 45$ deg, respectively, away from the forward stagnation line of the cylinder. He observed a modified behavior of $f_s$ and the flow structure. Using acoustic waves emitted from a slot on the surface of a cylinder, Hsiao and Shyu[13] demonstrated that a local perturbation near the shear-layer instability frequency and around the flow separation point caused an increase in lift but a reduction in drag and the vortex scale. In both investigations the acoustic excitation did not have any apparent relationship with vortex shedding.

The paper proposes an alternative to the existing open-loop control methods. A novel technique based on piezoelectric actuators is investigated. When placed within an electric field, the piezoelectric effect results in a strain in the material. Conventional piezoelectric wafers can only generate very small deformation. The piezoceramic actuator presently investigated overcomes this obstacle by embedding a piezoelectric layer on the surface of a curved metallic thin plate. Because of its special fabrication process and the effect of curvature, a relatively large displacement can be achieved. This actuator is further characterized by a light weight and is capable of generating large forces over a wide range of frequencies. When the actuator is used to create a perturbation on the surface of a bluff body, fluid dynamics or interactions between fluid and structure can be altered, thus modifying vortex shedding. This technique is found to be particularly effective for the control of vortices from a freely vibrating structure in response to flow excitation, especially when resonance occurs. Flow measurements using a laser-induced fluorescence (LIF) technique, particle image velocimetry (PIV), and hot wire indicate that the vortex strength can be drastically reduced or increased depending on the perturbation frequency. The corresponding variation in the crossflow distribution of Reynolds stresses is also measured using a two-component laser Doppler anemometer.

## II. Experimental Details

### A. Wind Tunnel and Test Cylinder

Experiments were conducted in a closed-circuit wind tunnel with a square working section ($0.6 \times 0.6$ m) of 2.4-m length. The wind speed of the working section is up to 50 m/s. The streamwise mean velocity uniformity is about 0.1%, and the turbulence intensity is less than 0.4%. More details of the tunnel were given in Zhou et al.[14] An aluminum alloy square cylinder of side $h = 0.0152$ m was mounted horizontally in the midplane, 0.2 m downstream of the exit plane of the contraction, and spanned the full width of the working section, resulting in a blockage of about 2.53%. The cylinder, supported on springs at both ends, was allowed to vibrate laterally (Fig. 1). Measurements were carried out on the resonance condition of the fluid-structure system, that is, $f_s \approx f_n'$ (=30 Hz). The corresponding reduced velocity $U_r (\equiv U_\infty / f_n' h)$ was about 7.8, $Re$ was $3.5 \times 10^3$, and the maximum displacement of cylinder $Y_{\max}$ was about 1.2 mm, or $0.08h$.

### B. Actuators and Their Installation

Piezoelectric actuators presently used were prestressed and curved; they consist of a number of composite laminates, which have different thermal expansion coefficients and deform out-of-plane under an applied voltage. Three actuators were embedded in series in a slot on one side of the cylinder to support a thin plastic plate of 3 mm thick, which was installed flush with the top cylinder surface (Fig. 2). To minimize the asymmetry of the dynamic system, the opposite side of the cylinder was identically constructed, but no actuators were installed. The length of the plastic plate was 0.49 m, that is, two-thirds of the cylinder length. The gap between the plastic plate and cylinder was very small, about 0.1 mm, and well lubricated. The plate flushes with cylinder surface, thus not changing the cross section of the cylinder. The actuators were activated by a signal generated from a signal generator and amplified by a dual-channel piezodriver amplifier (Trek PZD 700). Driven by the actuators, this plate would oscillate to create the local perturbation of the cylinder surface.

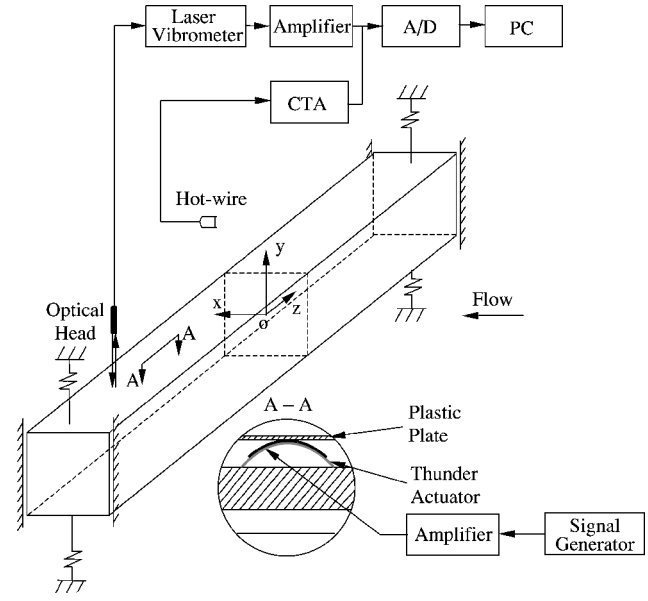


**Fig. 1 Experimental setup.**

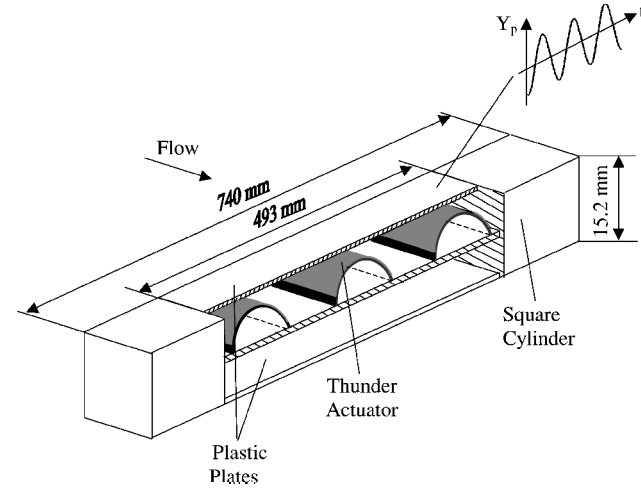


**Fig. 2 Installation of actuators in the square cylinder model. The drawing is not scaled to the actual size.**

Given a constant voltage, the deformation of actuators and subsequently the perturbation displacement $Y_p$ of the upper cylinder surface can vary with the perturbation frequency $f_p$. In the present investigation a constant rms voltage (141.4 V) was imposed on the actuators. At this voltage the $Y^*_{p,\mathrm{rms}} - f^*_p$ relationship (Fig. 3) was first quantified under no flow condition, where $f^*_p = f_p h / U_\infty$ and the rms value of the perturbation displacement, $Y^*_{p,\mathrm{rms}} = Y_{p,\mathrm{rms}}/h$. Unless otherwise stated, the asterisk denotes normalization by $U_\infty$ and $h$ in this paper. $Y_{p,\mathrm{rms}}$ exhibits a peak over a small range of $f^*_p$. The occurrence of the peak can be specified and is presently set over the range of $f^*_p = 0.1 \sim 0.13$. This range, once set, is not adjustable for the same actuators. The maximum $Y_{p,\mathrm{rms}}$ was 0.319 mm (or 0.021 $h$) at $f^*_p = 0.13$.

### C. Flowfield Measurements

The velocity field was measured using a Dantec standard PIV2100 system before and after the perturbation. Flow was seeded by smoke, which was generated from paraffin oil, of a particle size around 1 $\mu$m in diameter. Flow was illuminated in the plane of mean shear by two new wave standard pulsed laser sources of a wavelength of 532 nm, each having a maximum energy output of 120 mJ. Digital particle images were taken using one charge-coupled device (CCD) camera (HiSense Type 13; gain $\times$ 4, double frames, $1280 \times 1024$ pixels). A

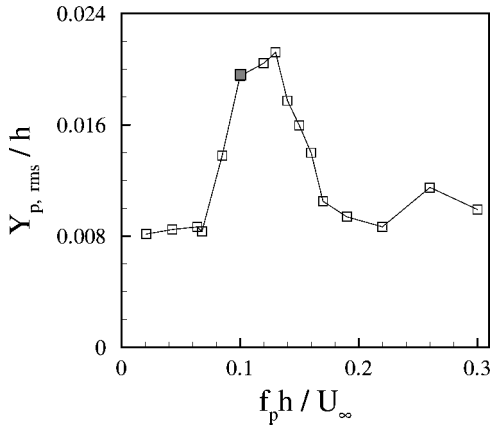


**Fig. 3 Dependence of the perturbation amplitude on the perturbation frequency under a constant voltage (no flow).**

Dantec FlowMap Processor (PIV2100 type) was used to synchronize image taking and illumination. A wide-angle lens was used so that each image covered an area of 150 × 120 mm of the flowfield, that is, $x/h \approx 0.8 \sim 10.8$ and $y/h \approx -2.7 \sim 5.2$; the $x$ and $y$ coordinates and their origin are defined in Fig. 1. The longitudinal and lateral image magnifications were identical, that is, 0.12 mm/pixel. Each laser pulse lasted 0.01 $\mu$s. The interval between two successive pulses was typically 50 $\mu$s. Thus, a particle would only travel 0.179 mm (1.53 pixels or 0.0118$h$) at $U_\infty = 3.576$ m/s, which was used for measurements. An optical filter was used to allow only the green light (wavelength = 532 nm) generated by a laser source to pass. In the image processing 32 × 32 rectangular interrogation areas were used. Each interrogation area included 32 pixels (≈0.25$h$) with 25% overlap with other areas in either the longitudinal or lateral direction. The ensuing in-plane velocity vector field consisted of 53 × 42 vectors. Spanwise vorticity component $\omega_z$ was approximately obtained based on particle velocities using a central difference scheme. The spatial resolution of vorticity estimate depends on grid spacing, about 2.9 mm or 0.19$h$.

The LIF measurement was conducted using the flow-visualization function of the PIV system. The same smoke as used in the PIV measurement was introduced through eight injection pinholes (diameter = 1 mm), symmetrically distributed at the midspan of the leading side (normal to the flow direction) of the cylinder. The CCD camera was used on the single-exposure mode. A wide-angle lens was also used to enlarge the view field so that each image covered an area of approximately 165 × 125 mm or $x/h \approx 0.33 \sim 11.2$ and $y/h \approx -4.1 \sim 4.1$ in the flow field. The recording interval between successive images was 0.143 s. Other configuration parameters were similar to the PIV measurement.

### D. Cylinder Displacement and Fluctuating Flow Velocity Measurements

A Polytec Series 3000 dual beam laser vibrometer[15] and a 5-$\mu$m tungsten hot wire were used to measure simultaneously the structural displacement and flow velocity, respectively. The hot wire, placed at $x/h = 2$ and $y/h = 1.5$, was operated at an overheat ratio of 1.8 with a constant temperature anemometer. Signals from both the laser vibrometer and the hot wire were conditioned and digitized using a 12-bit A/D board at a sampling frequency of 3.5 kHz per channel. The duration of each record was about 20 s.

The mean $\bar{U}$ and $\bar{V}$ and fluctuating velocities $u$ and $v$ along the $x$ and $y$ direction, respectively, in the wake ($x/h = 3 \sim 25$) were measured using a two-component laser Doppler anemometer (LDA) system (Dantec Model 58N40 with an enhanced flow velocity analyser signal processor). The measuring volume has a minor axis of 1.18 mm and a major axis of 2.48 mm. Thus, the measured mean velocity was estimated to have an error of less than 3%, and the corresponding error for the measured rms values $u_{rms}$ and $v_{rms}$ was less than 10%. The seeding was provided by smoke, the same as used in the PIV and LIF measurements.

## III. Perturbation Effects

### A. Impaired Vortex Strength

Figure 4 shows the photograph taken using the LIF technique when the fluid-structure system was under the resonance condition, that is, $f_s^* = f_n^{'*} = 0.13$ ($Re = 3.5 \times 10^3$, $U_r = 7.8$) without any external perturbation. The solid square in the figure indicates the cylinder position. The Kármán vortex street is evident. The isocontour (Fig. 5) of the normalized spanwise vorticity $\omega_z^* = \omega_z h / U_\infty$ from the PIV measurement show a similar flow pattern. The uncertainty of the vorticity measurement was estimated to be about 9%.

Once a perturbation was introduced at $f_p^* = 0.1$, however, the flow structure changed drastically, as shown in Fig. 6. The Kármán vortex street appears to be breaking up and greatly impaired irrespective of the phase of the cylinder oscillation. The quantitative information on the impaired vortex street can be gained from the contour of $\omega_z^*$ (Fig. 7). The magnitude $|\omega_{z\,\max}^*|$ of the maximum $\omega_z^*$ drops by about 46%. Furthermore, the size of vortices also shrinks significantly. The circulation around a vortex can be estimated by the following numerical integration[16]:

$$\frac{\Gamma}{U_\infty h} = \sum_{i,j} \left(\omega_z^*\right)_{ij} \frac{\Delta A}{h^2} \tag{1}$$

where $(\omega_z^*)_{ij}$ is spanwise vorticity over area $\Delta A = \Delta x \Delta y$ with $\Delta x$ and $\Delta y$ being the integral step along the $x$ and $y$ directions, respectively. Integration was conducted over an area enclosed by the cutoff level $|\omega_{zc}^*| = 0.4$, about 10% of $|\omega_{z\,\max}^*|$, as used by Sumner

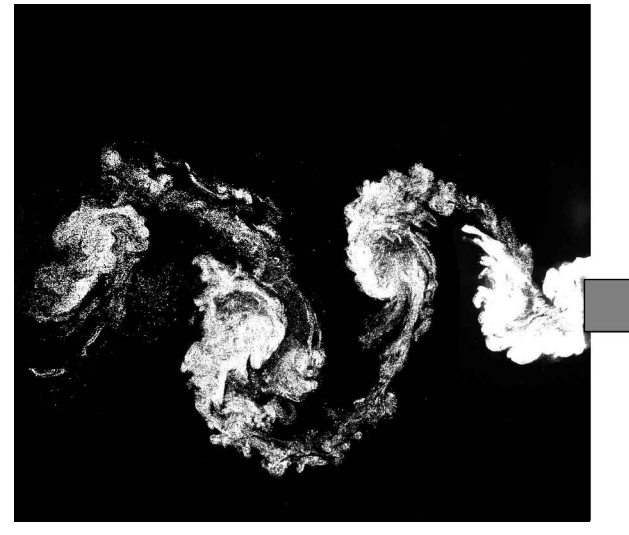

**Fig. 4 Typical photograph from LIF measurements of unperturbed vortex shedding ($f_p^* = 0$, $U_r = 7.8$, $Re = 3.5 \times 10^3$). Flow is right to left.**

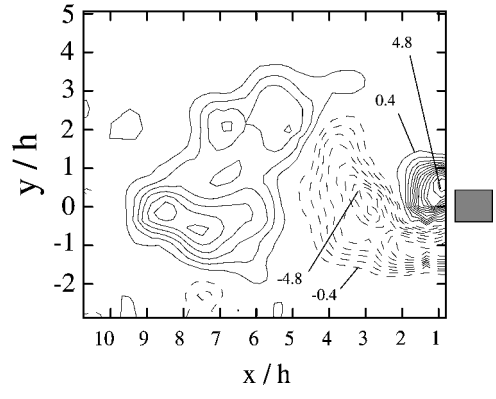


**Fig. 5 The isocontour of spanwise vorticity $\omega_z^* = \omega_z h/U_\infty$ from PIV measurements of unperturbed vortex shedding ($f_p^* = 0$, $U_r = 7.8$, $Re = 3.5 \times 10^3$): the contour increment $\Delta\omega_z^* = 0.4$; the cutoff level $|\omega_{zc}^*| = 0.4$. Flow is right to left.**

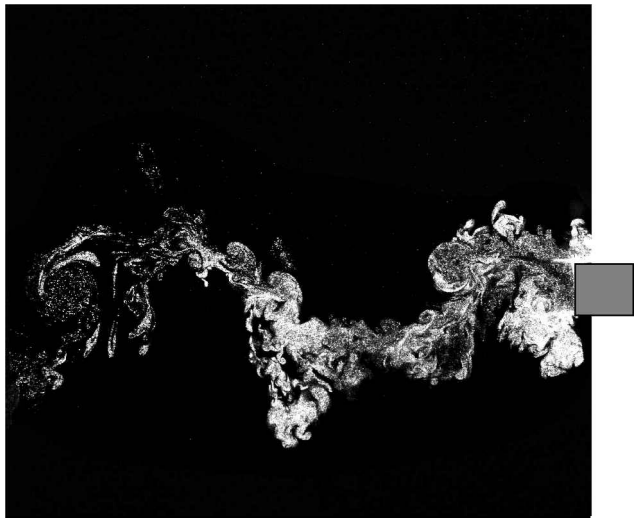

**Fig. 6 Typical photograph from LIF measurements of impaired vortex shedding ($f_p^* = 0.1$ is beyond the synchronization range, $U_r = 7.8$, $Re = 3.5 \times 10^3$). Flow is right to left.**

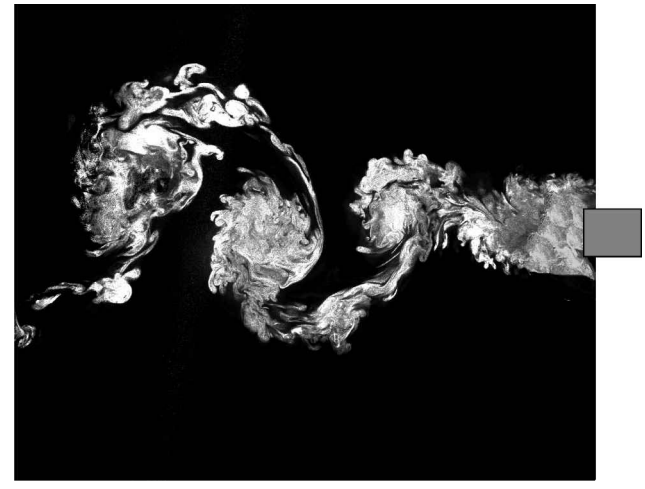

**Fig. 8 Typical photograph from LIF measurements of enhanced vortex shedding ($f_p^* = 0.13$ is within the synchronization range, $U_r = 7.8$, $Re = 3.5 \times 10^3$). Flow is right to left.**

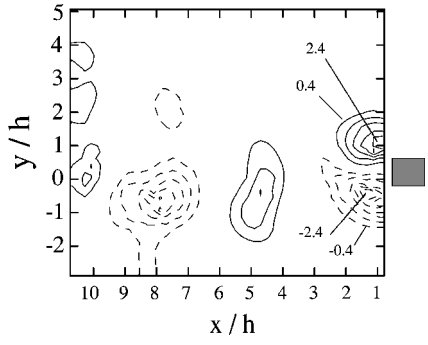


**Fig. 7 The isocontour of spanwise vorticity $\omega_z^* = \omega_z h / U_\infty$ from PIV measurements of impaired vortex shedding ($f_p^* = 0.1$ is beyond the synchronization range, $U_r = 7.8$, $Re = 3.5 \times 10^3$): the contour increment $\Delta\omega_z^* = 0.4$; the cutoff level $|\omega_{zc}^*| = 0.4$. Flow is right to left.**

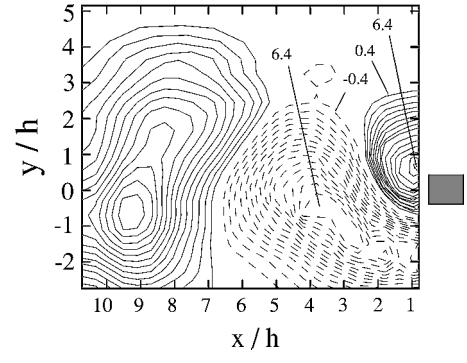


**Fig. 9 Isocontour of spanwise vorticity $\omega_z^* = \omega_z h / U_\infty$ from the PIV measurements of enhanced vortex shedding ($f_p^* = 0.13$ is within the synchronization range, $U_r = 7.8$, $Re = 3.5 \times 10^3$): the contour increment $\Delta\omega_z^* = 0.4$; the cutoff level $|\omega_{zc}^*| = 0.4$. Flow is right to left.**

et al.[17] The error associated with the $\Gamma$ estimate is about 15%. The decrease in $\Gamma$ exceeds 50%, compared with the case without perturbation (Fig. 5).

### B. Enhanced Vortex Strength

As the perturbation frequency was increased to $f_p^* = 0.13$, which coincided with the natural frequency of the fluid-cylinder system, the vortex shedding (Fig. 8) was enhanced. The vortices appear better organized and larger in size when compared with that without perturbation (Fig. 4). This is more evident in the contour of $\omega_z^*$ (Fig. 9). The magnitude of the maximum $\omega_z^*$ experiences a jump of 38%; the size enclosed by $|\omega_{zc}^*| = 0.4$ increases drastically (that is, Fig. 5). Accordingly, a conservative estimate of $\Gamma$ (part of the area enclosed by $|\omega_{zc}^*| = 0.4$ was outside the PIV image) doubles that in Fig. 5. Considering a relatively small perturbation amplitude $Y_{p,\mathrm{rms}}/h = 2\%$ ($Y_{\max}/h = 8\%$), the variation in the vortex street is astonishing, implying a great change in fluid-structure interactions during the vortex shedding process.

The surface perturbation was imposed only on the upper side of the square cylinder, but both sides of the wake centerline (Figs. 6–9) appear equally affected. The observation suggests that the local perturbation has changed the global interaction between fluid and structure.

## IV. Perturbed Fluid-Structure Interactions

It has been seen from Sec. III that $f_p^*$ is crucial in how the perturbation would influence the near wake and implicitly the fluid-structure interaction. To thoroughly understand the $f_p^*$ effect on fluid-structure interactions when synchronization ($f_s^* = f_n'^*$) occurs, the structural oscillation and streamwise fluctuating flow velocity were simultaneously measured using the laser vibrometer and a single hot wire (hot wire was located at $x/h = 2$ and $y/h = 1.5$), respectively, as $f_p^*$ varied from 0 to 0.34.

Figures 10a and 10b display the power spectral density functions $E_Y$ and $E_u$ of $Y$ and $u$, respectively. The spectrum of fluctuation $\alpha$ ($\alpha$ represents either $Y$ or $u$) has been normalized so that $\int_0^\infty E_\alpha(f)\,\mathrm{d}f = 1$. At $f_p^* = 0$ a pronounced peak occurs at $f_s^* = 0.13$ in both $E_Y$ and $E_u$, the number (0.91 in $E_Y$ and 0.59 in $E_u$) near the peak indicating the peak magnitude at $f_s^*$. The second harmonic is also evident at $f^* = 0.26$. Once the perturbation is introduced, both $E_Y$ and $E_u$ show an additional spike at $f_p^*$. For $f_p^* \leq 0.1$ the peak value at $f_s^*$ is attenuated for both $E_Y$ and $E_u$. The attenuation effect is most significant at $f_p^* = 0.1$, where the peak value in $E_Y$ and $E_u$ is only 25 and 40%, respectively, of its counterpart at $f_p^* = 0$. The result is consistent with the LIF and PIV measurements (Figs. 6 and 7). Note that the peak at the second harmonic is also appreciably reduced. As $f_p^*$ exceeds 0.13 but not beyond the second harmonic 0.26 of $f_s^*$, the peak at $f_s^*$ in $E_Y$ and $E_u$ is more pronounced than at $f_p^* = 0$; the maximum occurs at $f_p^* = 0.13$, where $f_p^* = f_s^* = f_n'^*$ and the peak value in both $E_Y$ and $E_u$ are more than twice the value at $f_p^* = 0$, agreeable with the LIF and PIV data (Figs. 8 and 9). But once $f_p^*$ reaches 0.3 and beyond, the peak value drops below that at $f_p^* = 0$. Evidently, the influence of the perturbation depends on the interrelationship between $f_p^*$ and $f_s^*$ or $f_n'^*$.

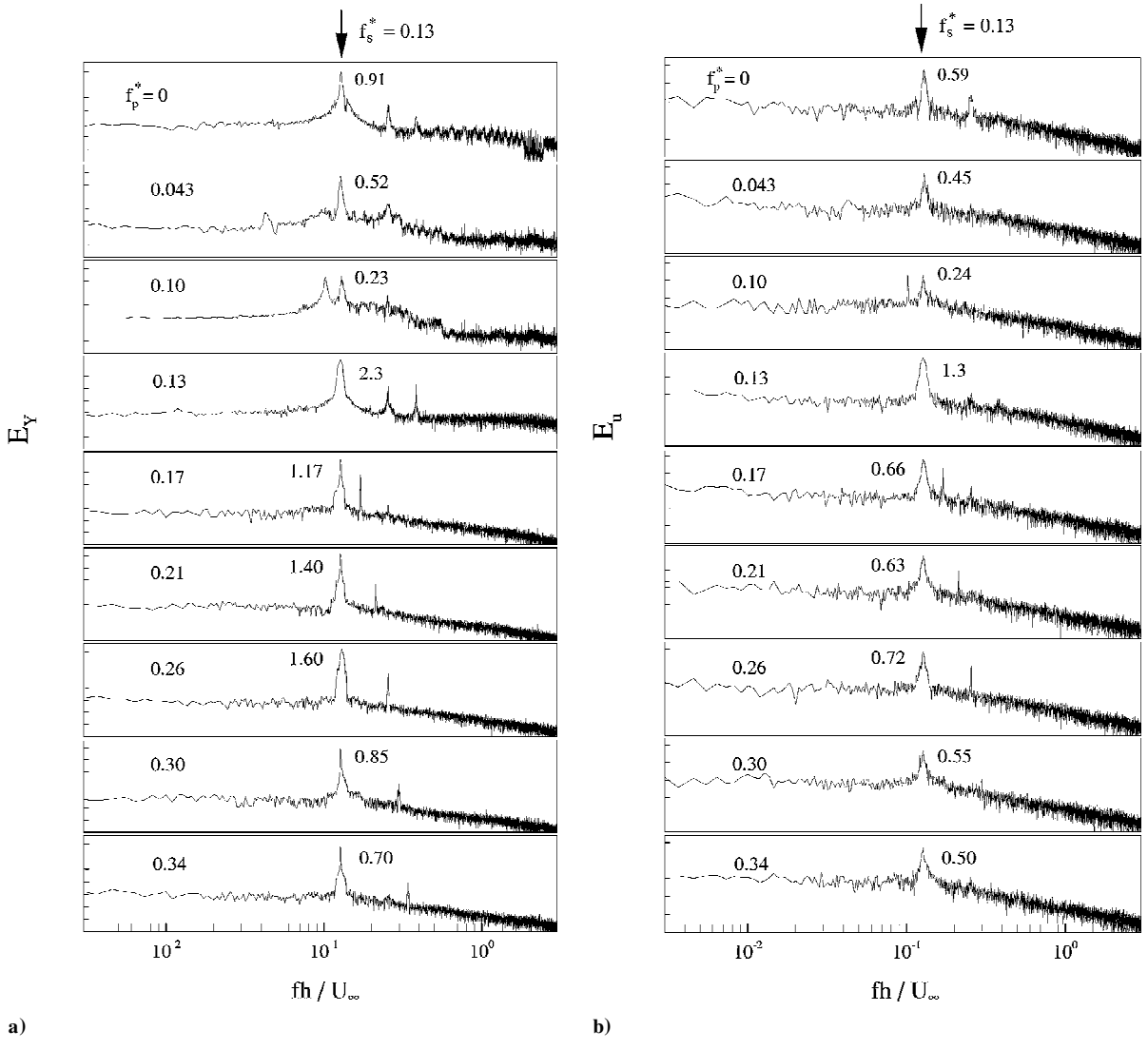


**Fig. 10 At various perturbation frequency $f_p^*$ a) power spectra of cylinder displacement $Y$ and b) fluctuating flow velocity $u$. The hot wire was located at $x/h = 2, y/h = 1.5$.**

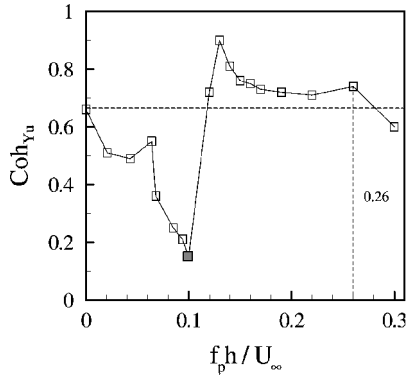


**Fig. 11 Effect of the perturbation frequency on the spectral coherence $Coh_{Yu}$ at $f_s^* \approx 0.13$ between the $Y$ and $u$ signals. The hot wire was located at $x/h = 2, y/h = 1.5$.**

The spectral coherence between $Y$ and $u$, calculated by $Coh_{Yu} = (Co_{Yu}^2 + Q_{Yu}^2)/E_Y E_u$, provides a measure of the degree of correlation between the Fourier components of $Y$ and $u$, where $Co_{Yu}$ and $Q_{Yu}$ are the cospectrum and quadrature spectrum of $Y$ and $u$, respectively. Here, the cross spectrum is computed from the Fourier transform of the correlation $\overline{Y(t+\tau)u(t)}$ (see Zhang et al.[18] for more details). Figure 11 presents $Coh_{Yu}$ at $f_s$ as $f_p^*$ varies. The perturbation causes an increase in $Coh_{Yu}$ at $f_s$, compared with that at $f_p^* = 0$, for $0.1 < f_p^* \leq 0.26$ and otherwise a decrease. The enhanced $Coh_{Yu}$ range can result from synchronization between vortex shedding and induced vibration. Based on experimental data, Gowda[19] suggested that for bluff bodies with fixed separation points the synchronization phenomenon began at $f_s \approx 0.8 f_n'$ and ended when $f_s \approx 2 f_n'$. This corresponds presently to a frequency range of $f_p^* = 0.11 \sim 0.26$, coinciding well with the range of enhanced $Coh_{Yu}$.

To gain a better insight into the relationship between the $Y$ and $u$ signals, $Co_{Yu}$ is examined in Fig. 12. A strong peak occurs at $f_s^*$, which is negative for $0 < f_p^* \leq 0.1$, positive for $0.1 < f_p^* \leq 0.26$, and negative again for $f_p^* > 0.26$. The peak indicates a good correlation between $Y$ and $u$ at $f_s^*$, whereas the positive and negative signs correspond to in phased and antiphased $Y$ and $u$ at $f_s^*$, respectively. The average phase shift between $Y$ and $u$ can be quantified by the spectral phase angle (Fig. 13), defined by $\phi_{Yu}[\equiv \tan^{-1}(Q_{Yu}/Co_{Yu})]$. This angle is zero at $f_p^* = 0$, close to $-\pi$ for $0 < f_p^* \leq 0.1$ and fluctuating about zero for $f_p^* > 0.1$.

An interpretation is now proposed for the enhancement and impairment of vortex shedding. As $f_p^*$ falls within the possible synchronization range, the perturbation will not break the synchronization between vortex shedding and structural vibration; instead, the perturbation is more likely to increase the strength of synchronization or resonance. Notably, at $f_p^* = 0.13$, where $f_n' = f_s = f_p$, $Coh_{Yu}$ at $f_s$ reaches the maximum 0.90. However, when $f_p^*$ is beyond the synchronization range the perturbation changes the phase relationship between synchronizing structural oscillation and vortex shedding from zero to near $-\pi$. This implies an alteration in the nature of

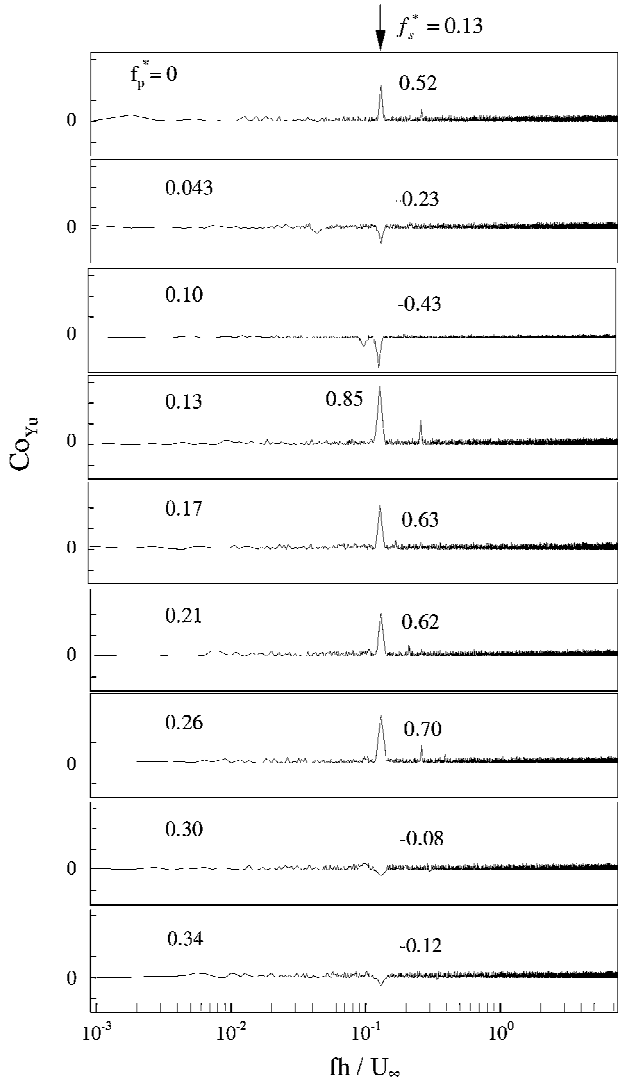


**Fig. 12 Cospectrum between the *Y* and *u* signals at various perturbation frequency $f_p^*$. The hot wire was located at *x/h* = 2, *y/h* = 1.5.**

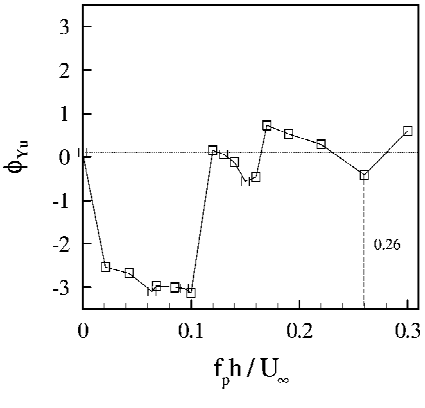


**Fig. 13 Effect of the perturbation frequency on the phase shift $\phi_{Yu}$ at $f_s^* \approx 0.13$ between the *Y* and *u* signals. The hot wire was located at *x/h* = 2, *y/h* = 1.5.**

fluid-structure interactions, the in-phased fluid excitation, and structural oscillation turning into antiphased interactions against each other, which dissipate each other in energy and result in drastic weakening vortex shedding and structural oscillation.

It is pertinent to comment that $Coh_{Yu}$ at $f_s$ drops to the minimum at $f_p^* = 0.1$ and reaches the maximum at $f_p^* = 0.13$. The perturbation effect is dependent on $Y_{p,\mathrm{rms}}$, as well as $f_p^*$. The $Y_{p,\mathrm{rms}}$ peak is presently set at $f_p^* = 0.1 \sim 0.13$ (Fig. 3). This might explain why

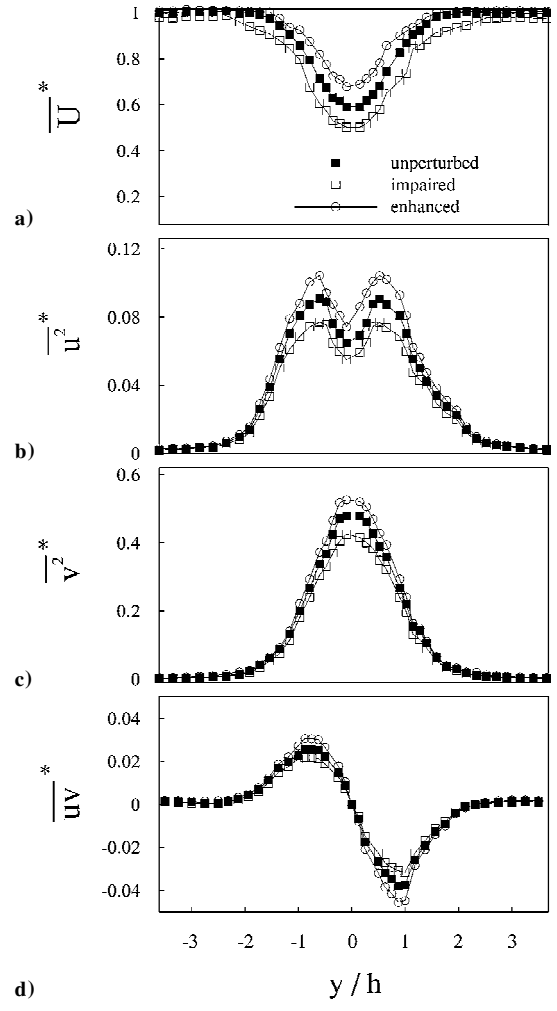


**Fig. 14 Crossflow distribution of mean velocity, Reynolds stresses at *x/h* = 3: a) $\overline{U}^*$, b) $\overline{u^2}^*$, c) $\overline{v^2}^*$ and d) $\overline{uv}^*$.**

the perturbation effect is particularly eminent in this $f_p^*$ range. The small $Y_{p,\mathrm{rms}}$ for $f_p^* = 0.02 \sim 0.07$ and $f_p^* \geq 0.26$ is at least partially responsible for the relatively weak perturbation effect over these frequencies (Fig. 11).

## V. Downstream Evolution of Perturbed Flow

It might be of fundamental interest to estimate how far downstream of the cylinder the perturbation effect could persist. This is investigated by examining the crossflow distribution of mean velocity $\overline{U}^*$ and Reynolds stresses $\overline{u^2}^*$, $\overline{v^2}^*$, and $\overline{uv}^*$, obtained from the LDA measurement. Figure 14 presents a comparison in $\overline{U}^*$, $\overline{u^2}^*$, $\overline{v^2}^*$, and $\overline{uv}^*$ at $x/h = 3$ between the cases without perturbation and the impaired ($f_p^* = 0.1$) or enhanced vortex street ($f_p^* = 0.13$). For $f_p^* = 0.1$ the maximum of $\overline{U}^*$, $\overline{u^2}^*$, $\overline{v^2}^*$, and $\overline{uv}^*$ at $x/h = 3$ shows a considerable decrease, down to 85, 85, 88, and 78% of that unperturbed, respectively. On the other hand, for $f_p^* = 0.13$ the four quantities increase by 16, 13, 10, and 22%, respectively. The results are in line with the LIF and PIV measurements. The perturbation on the upper side of the cylinder has the equal effect on either side of the wake centerline, as qualitatively seen from the vortex street (Figs. 6–9). The difference is still discernible at $x/h = 20$ but vanishes at $x/h = 25$ (not shown).

One remark is caused by the perturbation effect on the drag coefficient $C_D$, which can be estimated based on $\overline{U}^*$, $\overline{u^2}^*$, and $\overline{v^2}^*$ (Ref. 20), that is,

$$C_D = 2\int_{-\infty}^{\infty} \frac{\overline{U}}{U_\infty}\left(\frac{U_\infty - \overline{U}}{U_\infty}\right) \mathrm{d}\left(\frac{y}{h}\right) + 2\int_{-\infty}^{\infty} \left(\frac{\overline{v^2} - \overline{u^2}}{U_\infty^2}\right) \mathrm{d}\left(\frac{y}{h}\right) \tag{2}$$

Without perturbation $C_D$ is 1.88, falling in the range $(1.7 \sim 2.0)$ reported previously.[21–23] $C_D$ dropped marginally, about 5%, for the case of impaired vortex shedding ($f_p^* = 0.1$), but jumped by 17% when vortex shedding was enhanced ($f_p^* = 0.13$).

## VI. Conclusions

Piezoceramic actuators have been deployed to generate a perturbation of controllable frequency and amplitude on a square cylinder. The perturbation can be used for the effective control of vortex shedding from a bluff body in a crossflow. Investigation is conducted when a square cylinder and flow system experiences resonance, leading to the following conclusions:

1) When the perturbation frequency $f_p^*$ is outside the synchronization range of the fluid-cylinder system, the fluid-structure interaction has been altered so that vortex shedding and structural oscillation are anti-phased. The spectral coherence at $f_s$ drops from 0.66 ($f_p^* = 0$) to 0.15 ($f_p^* = 0.1$). Correspondingly, the vortex strength (circulation) reduces by 50%. The drag coefficient $C_D$ decreases slightly, only 5%.

2) When $f_p^*$ falls within the synchronization range of the fluid-cylinder system, vortex shedding and structural oscillation remain synchronized. As a matter of fact, the spectral coherence at $f_s$ increases substantially from 0.66 at $f_p^* = 0$ to 0.90 at $f_p^* = 0.13$. As a result, the vortex strength exceeds twice that at $f_p^* = 0$. There is an increase of 17% in $C_D$.

3) The perturbation also alters considerably the crossflow distribution of $\overline{U}^*$, $\overline{u^2}^*$, $\overline{v^2}^*$, and $\overline{uv}^*$. The maximum $\overline{U}^*$, $\overline{u^2}^*$, $\overline{v^2}^*$, and $\overline{uv}^*$ values at $x/h = 3$ drop by 14.6, 15.2, 12.1, and 22.0, respectively, in the attenuated vortex-shedding case and increase by 16.2, 13.0, 9.46, and 21.7%, respectively, in the enhanced vortex-shedding case. The perturbation effect persists up to $x/h \approx 25$.

## Acknowledgment

The authors acknowledge support given to them by the Central Research Grant of the Hong Kong Polytechnic University through Grant G-W108.

## References

[1]Berger, E., "Suppression of Vortex Shedding and Turbulence Behind Oscillating Cylinders," *Physics of Fluids*, Vol. 10, 1967, pp. 191–193.

[2]Warui, H. M., and Fujisawa, N., "Feedback Control of Vortex Shedding from a Circular Cylinder by Cross-Flow Cylinder Oscillations," *Experiments in Fluids*, Vol. 21, 1996, pp. 49–56.

[3]Fujisawa, N., Kawajiand, Y., and Ikemoto, K., "Feedback Control of Vortex Shedding from a Circular Cylinder by Rotational Oscillations," *Journal of Fluids and Structures*, Vol. 15, 2001, pp. 23–37.

[4]Fujisawa, N., and Nakabayashi, T., "Neural Network Control of Vortex Shedding from a Circular Cylinder Using Rotational Feedback Oscillations," *Journal of Fluids and Structures*, Vol. 16, 2002, pp. 113–119.

[5]Tokumaru, P. T., and Dimotakis, P. E., "Rotary Oscillation Control of a Cylinder Wake," *Journal of Fluid Mechanics*, Vol. 224, 1991, pp. 77–90.

[6]Shiels, D., and Leonard, A., "Investigation of a Drag Reduction on a Circular Cylinder in Rotary Oscillation," *Journal of Fluid Mechanics*, Vol. 431, 2001, pp. 297–322.

[7]Baz, A., and Ro, J., "Active Control of Flow-Induced Vibrations of a Flexible Cylinder Using Direct Velocity Feedback," *Journal of Sound and Vibration*, Vol. 146, 1991, pp. 33–45.

[8]Ffowcs-Williams, J. E., and Zhao, B. C., "The Active Control of Vortex Shedding," *Journal of Fluids and Structures*, Vol. 3, 1989, pp. 115–122.

[9]Roussopoulos, K., "Feedback Control of Vortex Shedding at Low Reynolds Numbers," *Journal of Fluid Mechanics*, Vol. 248, 1993, pp. 267–296.

[10]Lewit, M., "Active Control of Dipole Sound from Cylinders," *Proceedings of DAGA'92*, 1992.

[11]Huang, X. Y., "Feedback Control of Vortex Shedding from a Circular Cylinder," *Experiments in Fluids*, Vol. 20, 1996, pp. 218–224.

[12]Williams, D. R., Mansy, H., and Amato, C., "The Response and Symmetry Properties of a Cylindrical Wake Subjected to Localized Surface Excitation," *Journal of Fluid Mechanics*, Vol. 234, 1992, pp. 71–96.

[13]Hsiao, F. B., and Shyu, J. Y., "Influence of Internal Acoustic Excitation upon Flow Passing a Circular Cylinder," *Journal of Fluids and Structures*, Vol. 5, 1991, pp. 427–442.

[14]Zhou, Y., Zhang, H. J., and Liu, M. W., "The Turbulent Wake of Two Side-by-Side Circular Cylinders," *Journal of Fluid Mechanics*, Vol. 458, 2002, pp. 303–332.

[15]Zhou, Y., So, R. M. C., Jin, W., Xu, H. G., and Chan, P. K. C., "Dynamic Strain Measurements of a Circular Cylinder in a Cross Flow Using a Fibre Bragg Grating Sensor," *Experiments in Fluids*, Vol. 27, 1999, pp. 359–367.

[16]Cantwell, B., and Coles, D., "An Experimental Study of Entrainment and Transport in the Turbulent Near Wake of a Circular Cylinder," *Journal of Fluid Mechanics*, Vol. 136, 1983, pp. 321–374.

[17]Sumner, D., Price, S. J., and Païdoussis, M. P., "Flow-Pattern Identification for Two Staggered Circular Cylinders in Cross-Flow," *Journal of Fluid Mechanics*, Vol. 411, 2000, pp. 263–303.

[18]Zhang, H. J., Zhou, Y., and Antonia, R. A., "Longitudinal and Spanwise Structures in a Turbulent Wake," *Physics of Fluids*, Vol. 12, 2000, pp. 2954–2964.

[19]Gowda, B. H. L., "Some Measurements on the Phenomenon of Vortex Shedding and Induced Vibrations of Circular Cylinders," *Deutsche Luft-und Raumfahrt Forschungsbericht*, No. 75-01, 1975.

[20]Antonia, R. A., and Rajagopalan, S., "A Comment on the Determination of Drag of a Circular Cylinder," *AIAA Journal*, Vol. 28, 1990, pp. 1833–1835.

[21]Knisely, C. W., "Strouhal Numbers of Rectangular Cylinders at Incidence—A Review and New Data," *Journal of Fluids and Structures*, Vol. 4, 1990, pp. 371–393.

[22]Zhou, Y., and Antonia, R. A., "Effect of Initial Conditions on Vortices in a Turbulent Near Wake," *AIAA Journal*, Vol. 32, No. 6, 1994, pp. 1207–1213.

[23]Lee, B. E., "The Effect of Turbulence on the Surface Pressure Field of a Square Prism," *Journal of Fluid Mechanics*, Vol. 69, 1975, pp. 263–282.

W. J. Dahm
*Associate Editor*